*Superlattices and Microstructures, Vol. 23, No. 5, 1998*

# Light scattering by spin excitations in copper-oxide-based materials

M. J. KONSTANTINOVIĆ, Z. V. POPOVIĆ
*Institute of Physics, P.O. Box 57, 11001 Belgrade, Yugoslavia*

*(Received 7 July 1996)*

In this paper we present a study of spin dynamics in CuO, $Bi_2CuO_4$ and $CuGeO_3$ single crystals using Raman spectroscopy. The measurements of polarized Raman scattering spectra are performed in the temperature region from 10 to 300 K in various frequency ranges. We found and assigned the lines in the spectra that belong to magnetically ordered phases. The origin of these excitations, based on the temperature dependence of their energies, linewidths and symmetry arguments, is given. Also, we present calculations of two-magnon intensities, based on the densities of states, and compare them with experimental data.



## 1. Introduction

The discovery of high-temperature superconducting oxides produced a great interest in the investigation of the different properties of copper-oxide-based materials. Since the structure of the new superconducting materials is quite complex, a better understanding of their physical properties may come from the study of the simpler (less complex) structures that can be described as 'initial oxides' of high-temperature superconductors. We follow this general idea and focus our attention on copper-oxide-based materials that do not belong to the families of the insulating phases of high-temperature superconductors. In this paper we are mainly interested in the magnetic properties of these crystals, since almost all high-temperature CuO-based superconductors undergo an antiferromagnetic-superconducting phase transition upon doping. For a review see [1].

The insulating phases of the superconductors are well understood concerning the magnetic ordering. They show the existence of strong antiferromagnetically coupled CuO planes that are weakly interacting along the third direction.

Light scattering experiments are used to study the spin dynamics of such two-dimensional magnetic structures [2]. The results show quite unusual behaviour that is ascribed as coming from the low-dimensionality of the interaction combined with the quantum value of the spin $S = \frac{1}{2}$ [3]. The characteristic properties of the two-magnon scattering features observed by the Raman scattering technique (light scattering in antiferromagnets is dominated by spin-pair excitation [4]) are a spectral line-shape broadening compared with a calculation based on the two-magnon approximation and the appearance of scattering in forbidden geometries. Several different effects were proposed to explain these discrepancies: inclusion of quantum fluctuations [5] that are ignored in the two-magnon approximation, revision of the mechanism of the two-magnon–phonon decay process [6] and, most recently, inclusion of a resonant scattering process [7].

Besides studying the magnetic interactions in the insulating phase, we also investigated the effects of doping on the spin dynamics. All doped systems from insulating up to superconducting show appreciable spin fluctuations. These effects are observed by a number of experimental techniques [8]. Still, the importance

0749–6036/98/051131 + 11 $25.00/0 sm960587 

of such a magnetic interaction in the electron-pairing mechanism is not known and remains one of the most interesting problems in the physics of superconductors.

Here, we present a study of the spin dynamics in CuO, $Bi_2CuO_4$ and $CuGeO_3$ single crystals using Raman spectroscopy. Polarized Raman-scattering measurements are performed in the temperature region from 10 to 300 K in the various frequency ranges. We found and assigned the lines in the spectra that belong to magnetically ordered phases. The origin of these excitations based on the temperature dependences of their energies, linewidths and on symmetry arguments is given. Also, we present calculations of two-magnon intensities, and compare them with data.

## 2. Experimental details

The Raman spectra were excited by the 5145 and 4880 Å lines of an argon ion laser (the average power was about 100 mW). The light was focused onto a sample using a cylindrical lens. The experimental geometry was of a backscattering type with an aperture $f$ of the collective objective of 1:1.4. The scattered light was analysed using a Jobin Ivon monochromator, model U-1000, with 1800 grooves $mm^{-1}$ holographic gratings. As a detector, we used the Pelletier-effect cooled RCA 31034 A photomultiplier with a conventional photon-counting system. The samples were held in a closed-cycle Leybold cryostat, equipped with a low-temperature controller, Leybold model LTC-60, and evacuated by a turbopump.

## 3. Two-magnon approximation

In this section we outline the main steps in the calculation of the two-magnon intensities. The calculation of the magnon intensities is non-trivial, since the exact ground state and excited states of the Heisenberg hamiltonian are not known. The usual approximation is the replacement of the exact ground state by a Néel state together with an Anderson [9] linear approximation for treatment of the excited states. The starting point is writing down the Heisenberg hamiltonian in the form:

$$H = -\sum_{i,j} J_{i,j} \boldsymbol{S}_i \boldsymbol{S}_j + \text{ Anisotropy}, \tag{1}$$

where summation goes over all spins. For the moment we will not give the explicit form for the anisotropy terms, since they will be discussed for each type of structure we consider. The use of the linear approximation and the Holstein–Primakoff representation [10] leads, by applying the standard diagonalization procedure, to the spin-wave eigenvalues $\hbar\omega(\boldsymbol{k})$.

The second step for evaluating the two-magnon Raman intensities is the calculation of the correlation function $\langle(\chi_{\boldsymbol{k}}^{\alpha\beta})^*(\chi_{\boldsymbol{k}}^{\mu\nu})\rangle_\omega$. The angular brackets denote an average over the fluctuations and $\chi_{\boldsymbol{k}}^{\alpha\beta}$ are components of a susceptibility tensor with the form:

$$\chi^{\alpha,\beta}(\boldsymbol{r}) = \chi_0^{\alpha,\beta}(\boldsymbol{r}) + \sum_{\mu} K_{\alpha\beta,\mu}(\boldsymbol{r}) S_{\boldsymbol{r}}^{\mu} + \sum_{\mu,\nu} G_{\alpha\beta,\mu\nu}(\boldsymbol{r}) S_{\boldsymbol{r}}^{\mu} S_{\boldsymbol{r}}^{\nu} + \sum_{\boldsymbol{\delta}} \sum_{\mu\nu} H_{\alpha\beta,\mu\nu}(\boldsymbol{r}\boldsymbol{\delta}) S_{\boldsymbol{r}}^{\mu} S_{\boldsymbol{r}+\boldsymbol{\delta}}^{\nu} + \cdots \tag{2}$$

The first term is just the susceptibility in the absence of any magnetic excitations. The second two terms involve spin operators at a single ionic site $\boldsymbol{r}$ and in the scattering process they describe the one-magnon scattering. The last term in eqn (2) gives rise to two-magnon scattering in which a pair of magnons are created or destroyed. This term involves the product of spin operators at different ionic sites $\boldsymbol{r}$ and $\boldsymbol{\delta}$.

One of the simplest approaches for evaluating the correlation function is to use the Green's function formalism. From the Green's function equation of motion (for any two operators $X$ and $Y$):

$$\omega\langle\langle X; Y\rangle\rangle_\omega = \frac{1}{2\pi}\langle[X, Y]\rangle + \langle\langle[X, H]\rangle; Y\rangle_\omega, \tag{3}$$

and with the fluctuation-dissipation theorem:

$$\langle XY\rangle_\omega = -2[n(\omega)+1]\mathrm{Im}\langle\langle X;Y\rangle\rangle_\omega, \tag{4}$$

that relates the correlation function to the imaginary part of the corresponding Green's function, we can finally obtain the Green's function for the two-magnon process and corresponding differential cross-section. The two-magnon spectrum we calculate from a Green's function with the form [11]:

$$G(\boldsymbol{\delta},\boldsymbol{\delta}') = \langle\langle P(\boldsymbol{\delta});P(\boldsymbol{\delta})\rangle\rangle_\omega, \tag{5}$$

where $\boldsymbol{\delta}$ and $\boldsymbol{\delta}'$ are vectors connecting neighbouring spins and $P(\boldsymbol{\delta})$ is defined as:

$$P(\boldsymbol{\delta}) = \sum_{\boldsymbol{r}}^{x}(S^x_{\boldsymbol{r}}S^x_{\boldsymbol{r}+\boldsymbol{\delta}} + S^y_{\boldsymbol{r}}S^y_{\boldsymbol{r}+\boldsymbol{\delta}}). \tag{6}$$

Following the standard procedure [11], the two-magnon cross-section becomes proportional to:

$$I_{\text{two-magnon}} \sim \mathrm{Im}\left[\frac{G_0(\omega)}{1+bG_0(\omega)}\right], \tag{7}$$

where $G_0(\omega)$ corresponds to the non-interacting Green's function:

$$\mathrm{Im}G_0 = \mathrm{Im}\left[\frac{1}{N}\sum_{\boldsymbol{k}}\frac{\boldsymbol{\Phi}(\boldsymbol{k})}{\omega^2-4\omega^2(\boldsymbol{k})}\right] = \frac{\pi}{4N}\sum_{\boldsymbol{k}}\frac{\boldsymbol{\Phi}(\boldsymbol{k})}{\omega(\boldsymbol{k})}\delta(\omega-2\omega(\boldsymbol{k})), \tag{8}$$

and $b$ describes the strength of the magnon–magnon interaction. The $\boldsymbol{\Phi}(\boldsymbol{k})$ are weighting functions for different polarized configurations and their evaluation requires knowledge of the magnetic structure in the antiferromagnetic ordered phase. The symmetry factors in the case of $Bi_2CuO_4$ for different polarizations are [12]:

$$\Phi(\boldsymbol{k}) = \begin{cases} 4\cos^2(k_xa)\cos^2(k_ya) & \text{for } A_{1g} \\ 4\sin^2(k_xa)\sin^2(k_ya) & B_{1g} \\ 4\sin^2(k_xa)\cos^2(k_ya) & \text{for } E_g. \end{cases} \tag{9}$$

These functions are used in Section 4.2 for calculating the two-magnon light scattering intensities in $Bi_2CuO_4$.

## 4. Light scattering by spin excitation

### 4.1. CuO

There is special interest in the properties of the CuO crystal as it is incorporated in almost all high-$T_C$ materials. The CuO crystallizes in the monoclinic space group $C^6_{2h}$ and the whole three-dimensional network is built from two sets of chains $\infty^1[CuO_{4/2}]$ running along the [1,1,0] and [1,$\bar{1}$,0] directions [13]. The neutron scattering experiments showed antiferromagnetic ordering in CuO below 213 K [14], but a more careful analysis showed the existence of an incommensurate phase in the temperature region from 213 to 232 K [15]. The spin dynamics of this oxide is also studied using inelastic neutron diffraction measurements [16], as well as using Raman spectroscopy [17–22]. According to these results few modes appear when the crystal is cooled below the antiferromagnetic transition temperature. The Raman spectra of CuO single crystals were obtained in the (110) plane in the temperature region from 10 to 300 K in the spectral region from 200 to 800 $cm^{-1}$, Fig. 1. Three modes at frequencies 302, 352 and 634 $cm^{-1}$ correspond to phonon excitations and belong to $A_g$ and $2B_g$ symmetries, respectively. The mode at about 240 $cm^{-1}$ has a magnetic origin according to its frequency dependence as a function of the temperature [17], and is believed to belong to the scattering of the magnetic exciton, as its frequency cannot be reconciled with the spin-wave magnetic dispersion spectrum

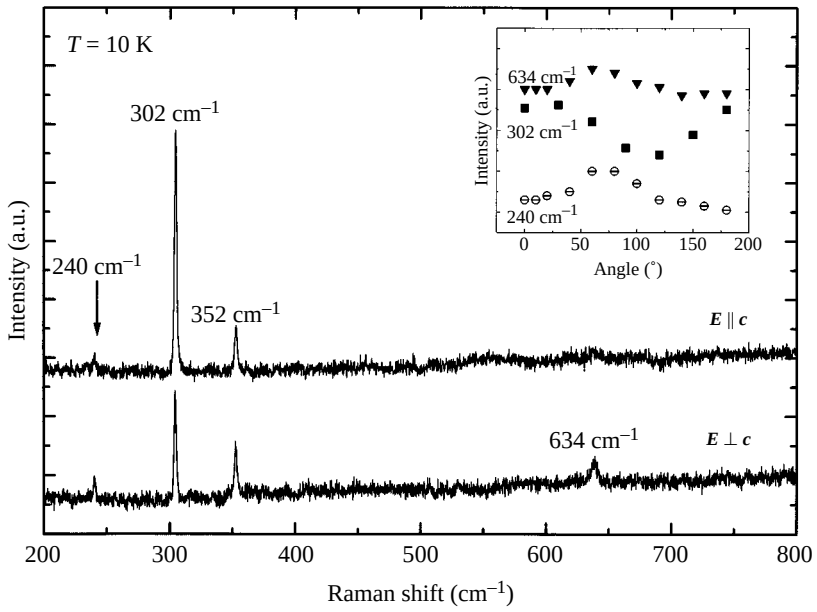


**Fig. 1.** The polarized Raman-scattering spectra of a CuO single crystal at a temperature of $T = 10$ K for two different incoming lights electric field vector orientations. Inset: The angle dependence of the mode intensities. The zero value of the angle corresponds to $\boldsymbol{E}\|\boldsymbol{c}$.

[15]. The symmetry of this mode is determined by analysing its intensity as a function of the angle between the incoming light's electric field vector and the *c*-axis. This dependence is given in the inset of Fig. 1. According to the analysis of the Raman scattering tensors obtained from the (110) plane [19, 21], trigonometric functional dependences are expected for the intensity dependences of the modes. From such dependences, Fig. 1, we assigned the 240 $cm^{-1}$ mode to the $B_g$ symmetry class.

Although the magnetic excitation Raman spectra does not give enough information for determining the exchange integrals, the neutron scattering studies [15] show the existence of the 3D antiferromagnetic interaction with the strong dominance of the magnetic superexchange interaction along the $[10\bar{1}]$ direction. The exchange integral associated with this direction is found to be around a value of $J = 80$ meV. The other two integrals are an order of magnitude smaller. It was also shown that the anisotropy term in the hamiltonian is not important as the experimental results do not display its signature.

### 4.2. $Bi_2CuO_4$

The properties of $Bi_2CuO_4$ have been extensively investigated in recent years as this crystal can be regarded as one of the possible 'impurity' phases in the Bi–Sr–Ca–Cu–O system. The crystal structure of $Bi_2CuO_4$ is tetragonal with isolated $CuO_4$ square planar units of $Cu^{2+}$ ions that are stacked on the top of each other in a staggered manner along the *c*-axis [23]. The $Bi_2CuO_4$ crystal exhibits 3D $S = \frac{1}{2}$, antiferromagnetic ordering below $T_N = 45$ K [24]. The spin waves were analysed using inelastic neutron scattering experiments [25] producing four superexchange constants, for fitting the magnon dispersion curves. The polarized Raman-scattering spectra [26] were measured in the spectral range between 10 and 640 $cm^{-1}$, at various temperatures between 10 and 300 K. The $T = 10$ K and $T = 300$ K spectra in $xx$, $xy$, $x'z$ and $zz$ polarized configurations are presented in Fig. 2. The complete assignments of the observed modes have already been given in [27]. The broad dominant feature observed in $xx$ and $x'z$ spectra, we assigned to a two-magnon mode because of

its frequency dependence as a function of temperature and magnon symmetry selection rules [28]. The small peak denoted by an arrow in Fig. 2, for $x'z$ polarization, comes from one-magnon scattering [27]. Since the one-magnon process gives the Brillouin-zone-center magnon frequency and the two-magnon process receives its strongest contribution from the zone-edge magnons, we made a comparison between the features of the scattered light spectrum and the magnon dispersion relation.

We used the Heisenberg anisotropy exchange hamiltonian [12] in order to calculate the spin-wave dispersion and the two-magnon density of states. We obtained the expression:

$$\hbar\omega(\boldsymbol{k}) = 2S\sqrt{(\mu + J_{11}(\boldsymbol{k}))^2 - (J_{12}(\boldsymbol{k}))^2} \tag{10}$$

where:

$$\begin{aligned}
\mu &= (J_{12}(0) + D_{12}(0) - J_{11}(0) - D_{11}(0)),\\
J_{11}(\boldsymbol{J}) &= 2J_1\cos(\boldsymbol{k}\cdot\boldsymbol{c}),\\
J_{12}(\boldsymbol{k}) &= 4\cos\left(\frac{\boldsymbol{k}\cdot\boldsymbol{a}}{2}\right)\cos\left(\frac{\boldsymbol{k}\cdot\boldsymbol{b}}{2}\right)\sqrt{(J_2 + (J_3 + J_4)\cos(\boldsymbol{k}\cdot\boldsymbol{c}))^2 + ((J_4 - J_3)\sin(\boldsymbol{k}\cdot\boldsymbol{c}))^2},
\end{aligned}$$

and

$$D_{11}(0) = 2D_1, \quad D_{12}(0) = 4(D_2 + D_3 + D_4). \tag{11}$$

The result of a two-magnon density of states (DOS) calculation is based on the above expressions and eqn (9) and is presented in Figs 3 and 4. The evaluation of the two-magnon intensities is done using numerical integration [12] and the results are presented in Figs 3 and 4 in the case of $B_{1g}$ and $E_g$ polarization configurations.

The values of the exchange integrals are obtained by simultaneous fit of the neutron and Raman-scattering data, and they are included in Fig. 3. According to the experiment, the $A_{1g}$ polarization configuration, although allowed by the selection rules [28] gives no noticeable two-magnon scattering, as the dominant contribution of this type of scattering comes from the centre of the Brillouin zone (where there is a low two-magnon DOS). The agreement between theory and experiment is both qualitative and quantitative, which suggest that the two-magnon scattering spectra can be completely described using interacting spin-wave theory, although the linear approximation is not rigorously applicable for spin $S = \frac{1}{2}$. The values of the exchange integrals we obtained are close to the values obtained by other authors [26, 29] but the essential degeneracy of the magnon branches is not produced by their results.

### 4.3. $CuGeO_3$

The most recent discovery of the first inorganic material $CuGeO_3$ with a spin–Peierls (SP) transition [30] provoked the re-examination of excitations in low-dimensional structures. The spin–Peierls transition, occurring at $T = 14$ K, is followed by opening of a gap in the excitation spectra due to magnetoelastic coupling, even though the 1D Heisenberg antiferromagnetic system has a gapless excitation spectra. The structure of the $CuGeO_3$ crystal is orthorhombic and the basic building blocks are corner-sharing $GeO_4$ tetrahedra that forms chains along the $c$-axis. The Cu atoms are surrounded by six O atoms, forming strongly deformed $CuO_6$ octahedra [31]. The Raman spectra of $CuGeO_3$ single crystals are measured [32–37] and unique spectra concerning the magnetic excitations are obtained. At the temperatures below the SP transition, besides phonon excitation, new peaks due to magnetic ordering appear. They are described as magnon-like excitations coming from energy-gap-pair excitations in the centre and at the edge of the Brillouin zone [37] with the value of exchange integral along the $c$-direction of $J = 5.3$ meV. These results are in good agreement with the inelastic neutron scattering measurements [38, 39]. Above the SP transition, in the short-range-ordering regime, from $T = T_{SP}$ to $T \approx 60$ K, a very broad continuum is observed; see Fig. 5. These excitations are usually described

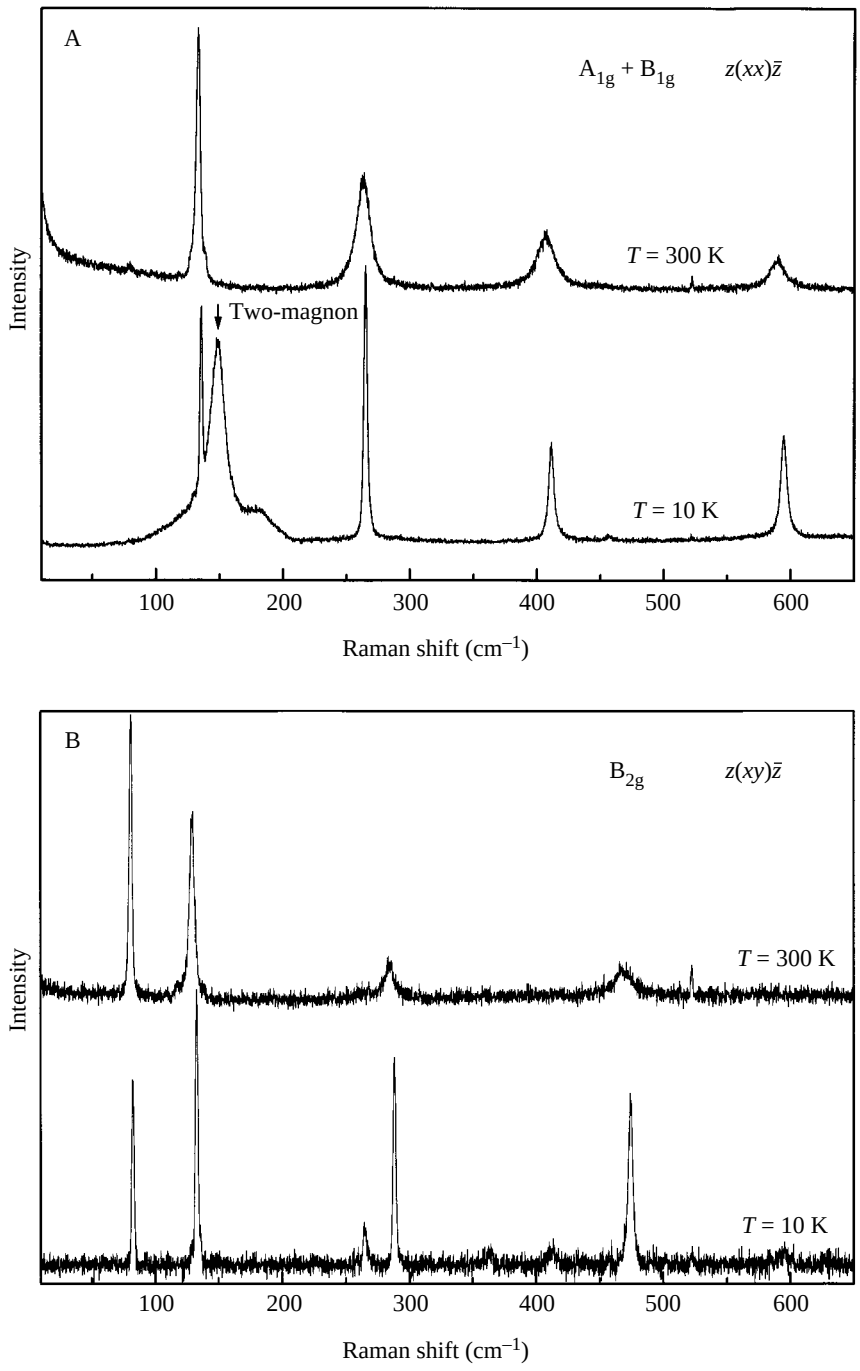


**Fig. 2.** The Raman scattering spectra of $Bi_2CuO_4$ at various temperatures in $xx$, $xy$, $x'z$ and $zz$ polarization configurations.

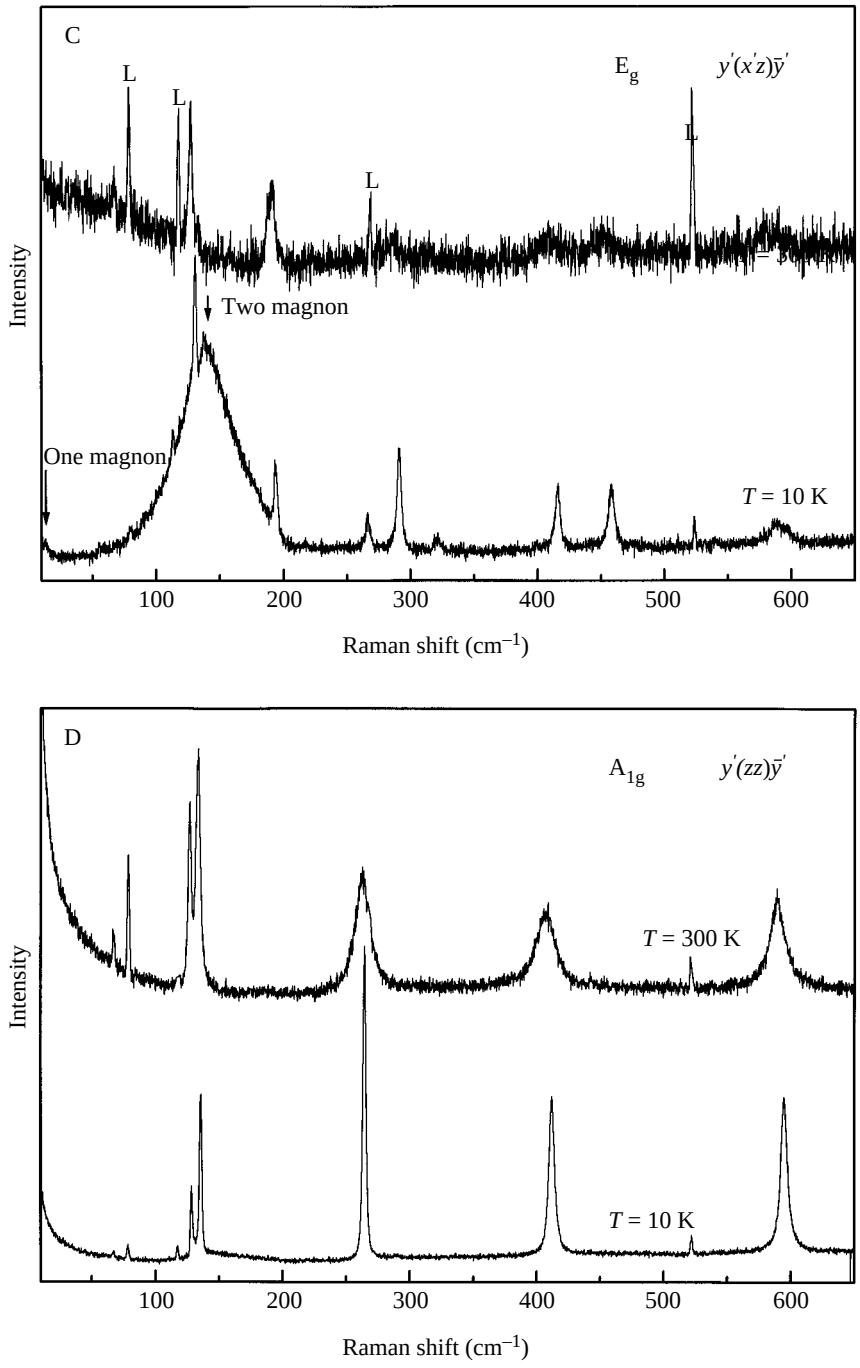


**Fig. 2.** Continued.

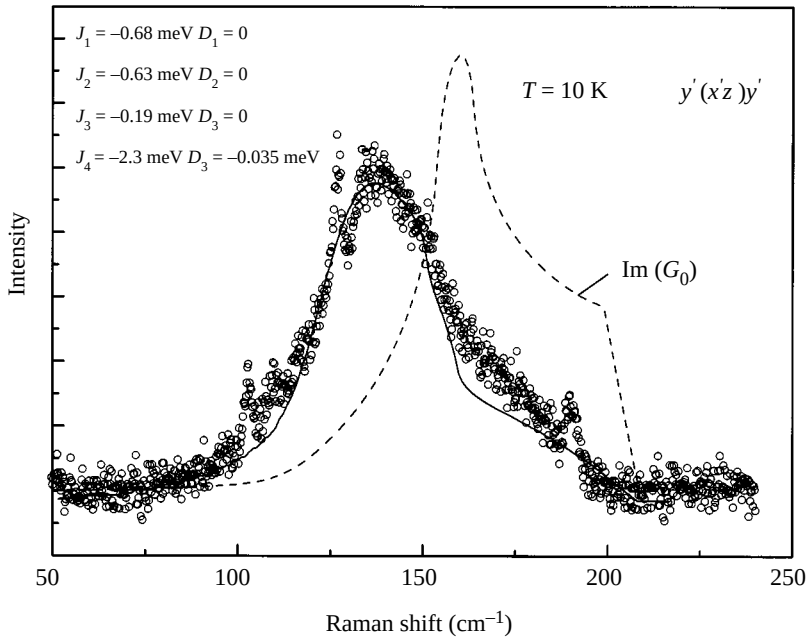


**Fig. 3.** The Raman scattering spectra of $Bi_2CuO_4$ at a temperature of $T = 10$ K in the $y'(x'z)y'$ polarization configuration together with two-magnon intensity calculation curves (full and dashed). Inset: The values of the exchange integrals obtained from the fit.

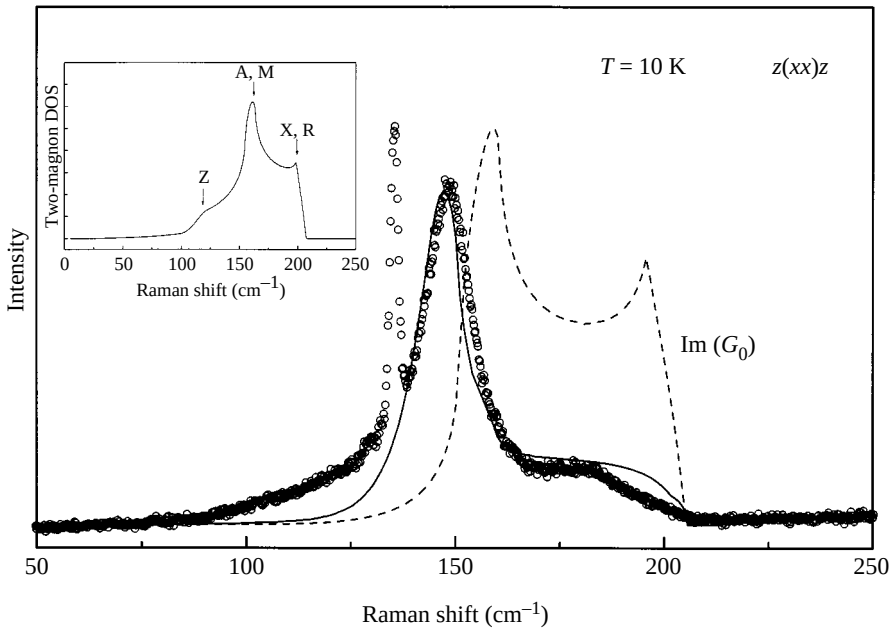


**Fig. 4.** The Raman scattering spectra of $Bi_2CuO_4$ at a temperature of $T = 10$ K in the $z(xx)z$ polarization configuration together with two-magnon intensity calculation curves (full and dashed). Inset: Two-magnon density of states.

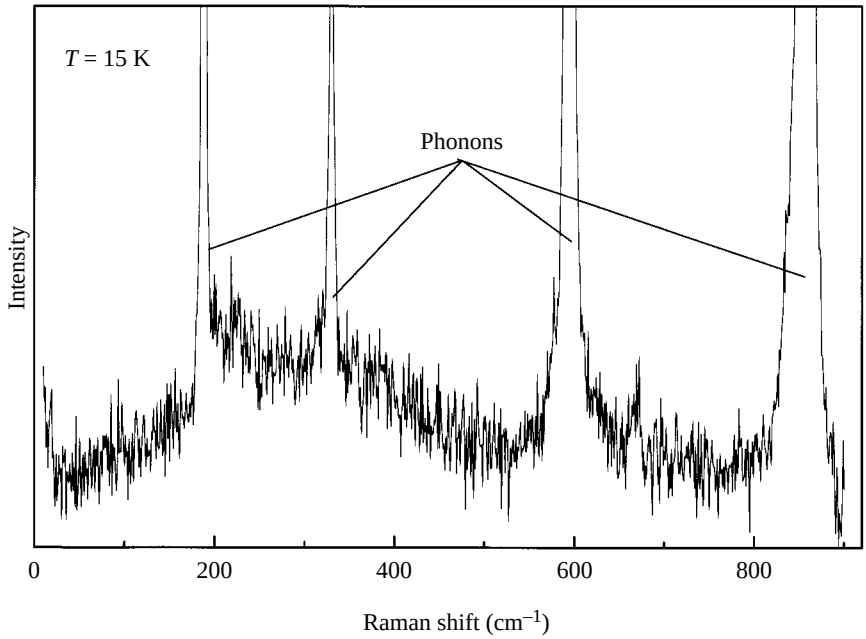


**Fig. 5.** The Raman scattering spectra of $CuGeO_3$ at a temperature of $T = 15$ K in the $yy$ polarization configuration.

as coming from fluctuations of the magnetic moments that are important in this quantum system, $S = \frac{1}{2}$. Unfortunately, the calculation does not fit the feature very well [37] and so the origin of this broad excitation spectrum is still under investigation.

## 5. Concluding remarks

Although the crystals we studied here started to be interesting because of the relevance to high-$T_C$ superconducting materials, their optical properties are very interesting in their own right. It is still not clear what is so important inside the layered structure of Cu–O planes that makes hole–superconducting pairing possible at high temperatures, but it is believed that the answer is hidden somewhere inside the unique low-dimensional properties of these crystals. Indeed some authors believe that Cu–O planes are not needed for high-$T_C$ superconductivity, and classify $Ba_{1-a}K_aPb_{1-b}Bi_bO_3$ as such a material.

Nevertheless, from this study, we found that the Cu–O structure incorporated in some materials may give quite a unique variety of phenomena, from low-dimensional-type interactions up to almost textbook examples of their optical properties.

The CuO crystal exhibits the layered structure that is usually formed in high-$T_C$ materials and it is antiferromagnetic concerning the magnetic interaction but the optical spectra are not very rich with observable excitations. Still there is a huge interaction between phonon and magnetic systems, according to the IR measurements. Hence, these crystals require special attention and further study.

The $Bi_2CuO_4$ crystal exhibits 3D antiferromagnetic ordering with excitation spectra that can be completely described using interacting, linear spin-wave theory, although the linear approximation is not rigorously applicable for a system with spin $S = \frac{1}{2}$.

Finally, the $CuGeO_3$ crystal is the first inorganic material that exhibits one-dimensional magnetic ordering

with a Peierls instability. Concerning the magnetic interaction, the question about excitation spectra above the spin–Peierls transition temperature is still open.

*Acknowledgement*—This work was supported by the Serbian Ministry of Science and Technology under project 01E09.

## References

[1] P. W. Anderson, Science **235**, 1196 (1987).
[2] M. Cardona and G. Gunterodt (eds), *Light Scattering in Solids VI* (Springer, Berlin, 1991).
[3] R. R. P. Singh, Comm. Condens. Mat. Phys. **15**, 241 (1991).
[4] P. Fleury and R. Loudon, Phys. Rev. **166**, 514 (1968).
[5] R. R. P. Singh, P. A. Fleury, K. B. Lyons, and P. E. Sulewski, Phys. Rev. Lett. **62**, 2736 (1989).
[6] D. Knoll, C. Thomsen, M. Cardona, and P. Murugaraj, Phys. Rev. **B42**, 4842 (1990).
[7] G. Blumberg, P. Abbamonte, M. V. Klein, W. C. Lee, D. M. Ginsberg, L. L. Miller, and A. Zibold, Phys. Rev. **B53**, R11930 (1996).
[8] See *High Temperature Superconductivity* Proc. Los Alamos Symp., edited by K. S. Bedel, (1989).
[9] P. W. Anderson, Phys. Rev. **86**, 694 (1952).
[10] T. Holstein and H. Primakoff, Phys. Rev. **58**, 1098 (1940).
[11] R. J. Elliot and M. F. Thorpe, J. Phys. **C2**, 1630 (1969).
[12] M. J. Konstantinović, Z. Konstantinović, and Z. V. Popović, Phys. Rev. **B54**, 68 (1996).
[13] S. Asbrink and L. J. Norrby, Acta Crystallogr. **B26**, 8 (1970).
[14] B. X. Yang, J. M. Tranquada, and G. Shirane, Phys. Rev. **B38**, 174 (1988).
[15] M. Ain, A. Menelle, B. M. Wanklyn, and E. F. Bertaut, J. Phys. Condens. Matter **4**, 5327 (1992).
[16] M. Ain, W. Reichardt, B. Hennion, G. Pepy, and B. M. Wanklyn, Physica **C162–164**, 1297 (1989).
[17] J. Chrzanowski and J. C. Irwin, Solid State Commun. **70**, 11 (1989).
[18] J. Chrzanowski, J. C. Irwin, T. Wei, and D. J. Lockwood, Physica **C166**, 456 (1990).
[19] H. F. Goldstein, D.-S. Kim, P. Y. Yu, and L. C. Bourne, Phys. Rev. **B41**, 7192 (1990).
[20] S. Guha, D. Peebles, and T. J. Wieting, Phys. Rev. **B43**, 13092 (1991).
[21] G. Kliche and Z. V. Popović, Phys. Rev. **B42**, 10060 (1990).
[22] Z. V. Popović, M. J. Konstantinović, and W. Konig, Proc. 13th Gen. Conf. EPS, Condens. Mat. Division, Regensburg p. 1384 (1993).
[23] J. C. Boivin, D. Tomas, and S. Tridot, C. R. Acad. Sci. **C276**, 1195 (1973).
[24] E. W. Ong, K. H. Kwei, R. A. Robinson, B. L. Ramakrishna, and R. B. von Dreele, Phys. Rev. **B42**, 4225 (1990).
[25] K. Yamada, K. Takada, S. Hosoya, Y. Watanabe, Y. Endoh, N. Tomonaga, T. Suzuki, T. Ishikagi, T. Kamijama, H. Asano, and F. Izumi, J. Phys. Soc. Japan **20**, 2406 (1991).
[26] M. Ain, G. Dhalenne, O. Guiselin, B. Hennion, and A. Revcolevschi, Phys. Rev. **B47**, 8167 (1993).
[27] M. J. Konstantinović, Z. V. Popović, S. D. Dević, A. Revcolevschi, and G. Dhalenne, J. Phys. Condens. Matter **4**, 7913 (1992).
[28] M. J. Konstantinović and Z. V. Popović, J. Phys. Condens. Matter **6**, 10357 (1994).
[29] K. Murayama, K. Saikawa, and K. Motizuki, J. Fac. Sci. Shinshu Univ. **29**, 9 (1994).
[30] M. Hase, I. Terasaki, and K. Uchinoqura, Phys. Rev. Lett. **70**, 3651 (1993).
[31] H. Völlenkle, A. Wittmann, and H. Nowotny, Monat. Chem. **98**, 1352 (1967).
[32] S. Sugai, J. Phys. Soc. Japan **62**, 3829 (1993).
[33] S. D. Dević, M. J. Konstantinović, Z. V. Popović, G. Dhalenne, and A. Revcolevschi, J. Phys. Condens. Matt. **6**, L745 (1994).
[34] M. Udagawa, H. Aoki, N. Ogita, O. Fujita, A. Sohma, A. Ogihara, and J. Akimitsu, J. Phys. Soc. Japan **63**, 4060 (1994).

[35] H. Kuroe, T. Sekine, M. Hase, Y. Sasago, K. Uchinokura, H. Kojima, I. Tanaka, and Yoshibuya, Phys. Rev. **B50**, 16469 (1994).
[36] Z. V. Popović, S. D. Dević, V. N. Popov, G. Dhalenne, and A. Revcolevschi, Phys. Rev. **B52**, 4185 (1995).
[37] P. H. M. van Loosdrecht, J. P. Boucher, G. Martinez, G. Dhalenne, and A. Revcilevchi, Phys. Rev. Lett. **76**, 311 (1996).
[38] L. P. Regnault, M. Ain, B. Hennion, G. Dhalenne, and A. Revcolevschi, Phys. Rev. **B53**, 5579 (1996).
[39] M. Nishi, O. Fujita, and J. Akimitsu, Phys. Rev. **B50**, 6508 (1994).